A methodology to develop part acceptance criteria model using non-destructive inspection technique for FDM printed part

Feng Lin Ng*, Thang Q. Tran, Tong Liu

Singapore Institute of Manufacturing Technology, 5 CleanTech Loop #01-01, CleanTech Two Block B, Singapore 636732, Singapore

Abstract

Additive Manufacturing (AM) has transit over the years from simple prototyping to high-mix-low-volume production. Sectors such as Aerospace or Biomedical that have adopted Additive Manufacturing for parts production have stringent requirement for strength and minimal tolerance for sub-surface defects. The presence of embedded defects usually leads to premature failure and additional cost for reinstallation. The current gold standard for Non-Destructive Inspection (NDI) technique is the use of 3D micro-CT scan. 3D micro-CT scan although provide the best resolution for defect detection, it is expensive, time consuming and laborious. The defects found in polymer 3D printed component, e.g., Fused Deposition Modeling, may not require high resolution imaging for defect detection due to the nature of printing process. Therefore, 2D X-ray imaging known for its short imaging and processing time has been used in this study with Acrylonitrile Butadiene Styrene (ABS) as the model material. Defects of various void sizes were introduced to tensile test coupons to determine the effect of void sizes on tensile properties. Good linear agreement (R2 = 0.998) has been observed between the void sizes and tensile strength which was then used to develop the part acceptance criteria model. The part acceptance criteria model developed from 2D X-ray imaging and mechanical test data suggest the feasibility of using such methodology to perform quality checks on 3D printed part which obviates the need for time consuming 3D micro-CT scans and unsustainable destructive testing.

1. Introduction

Fused Deposition Modeling (FDM) is a widely used additive manufacturing (AM) method for 3D printing of polymers due to its ease of handling, cost effectiveness and wide range of materials availability. To build a part using FDM process, a solid polymer filament is unwounded from a spool and fed through a heated extruder. The filament is then heated up to its melting temperature where the molten plastic material is extruded through the nozzle of certain diameter. As the extruder head move according to the digital model data of the fabricated part, the extruded melt material is deposited on a print bed. The polymeric material will solidify rapidly and adhere with the surrounding material to form the printed part. After the build of the corresponding layer is completed, either the extruder head or the print bed moves to an appropriate layer height. This is followed by the deposition of a new layer on the previous one until the part is completely built.

Due to the layer-by-layer deposition process, FDM printed parts always possess inherent voids and gaps in their internal structure [1]. The voids and gaps result in poor bonding between successive rasters within a layer or between successive layers. The effect of inherent voids and gaps is magnified if the printed part is subjected to a load perpendicular to the printed layers [2]. According to 3D micro-CT scan result reported by [3], most inherent voids in FDM printed parts have diameter in the range between 0.1 and 1 mm while the part porosity can be as high as 10 % [3]. These inherent features can be considered as acceptable defects but those with diameter larger than 1 mm should be treated with caution. Besides, defects such as delamination, voids, inclusions, sub-surface defects, and non-colinear deposition could be formed by imprecise machine positioning, environmental changes, feedstock variability and nozzle clogs [3]. These defects could cause decreased mechanical properties and possible part failure. Therefore, it is crucial to detect these unacceptable defects for quality control, especially for sub-surface defects.

Quality control is a necessary process to ensure defect-free final products in manufacturing, this is especially necessary for sectors with stringent requirements. While destructive testing of a small number of product samples is widely used in large volume mass production for quality checks, this approach is not viable for AM technology [4]. This is because the cost of destructive testing in large volume mass production processes is usually low as only small percentage of the parts are tested under statistical process control. However, for AM technology, destructive testing is not effective since adopters of AM techniques usually leverage the benefits of AM for high-mix-low-volume production. The parts printed by AM could be of a more complicated design which could make the quality assessment more complex hence more expensive compared to conventional techniques. As a result, expensive 3D micro-CT scan is still the current gold standard for defect detection in AM printed parts despite being expensive, time consuming and laborious [5]. Therefore, in this study 2D X-ray imaging was adopted to determine the feasibility of capturing sub-surface defects in FDM printed parts. Controlled embedded defects were introduced to tensile test coupons where the corresponding mechanical strength was determined and used to develop an acceptance criteria model. The developed methodology thus provides AM users an alternative technique for product quality checks which is less costly, time-consuming and more sustainable since no destructive testing of products will be required.

2. Methodology

2.1. FDM printing of ABS tensile test coupons

The Stratasys Fortus 400mc system was used in this study to 3D print test coupons for acceptance criteria model development. ASTM D638 Type I tensile coupon was used for this development as it enabled the direct characterization of parts with embedded defects. Acrylonitrile Butadiene Styrene (ABS) material, M30, was purchased from Stratasys and used in this study as model material. A T16 (0.254 mm) nozzle was used for the printing of model material and T12SR (0.178 mm) nozzle was used for the printing of support material. Insight 14.4 software was employed to generate toolpath required for the printer based on computer aided design (CAD) model. The tensile coupons were printed in an upright Z orientation (Fig. 1) to characterize the resultant Z-strength as a result of embedded defects. The tensile coupons were printed at an infill angles of [+45°/-45°] and layer thickness of 0.254 mm. A printing temperature of 316 °C and enclosed chamber temperature of 98 °C were employed as default settings for ABS-M30 material.

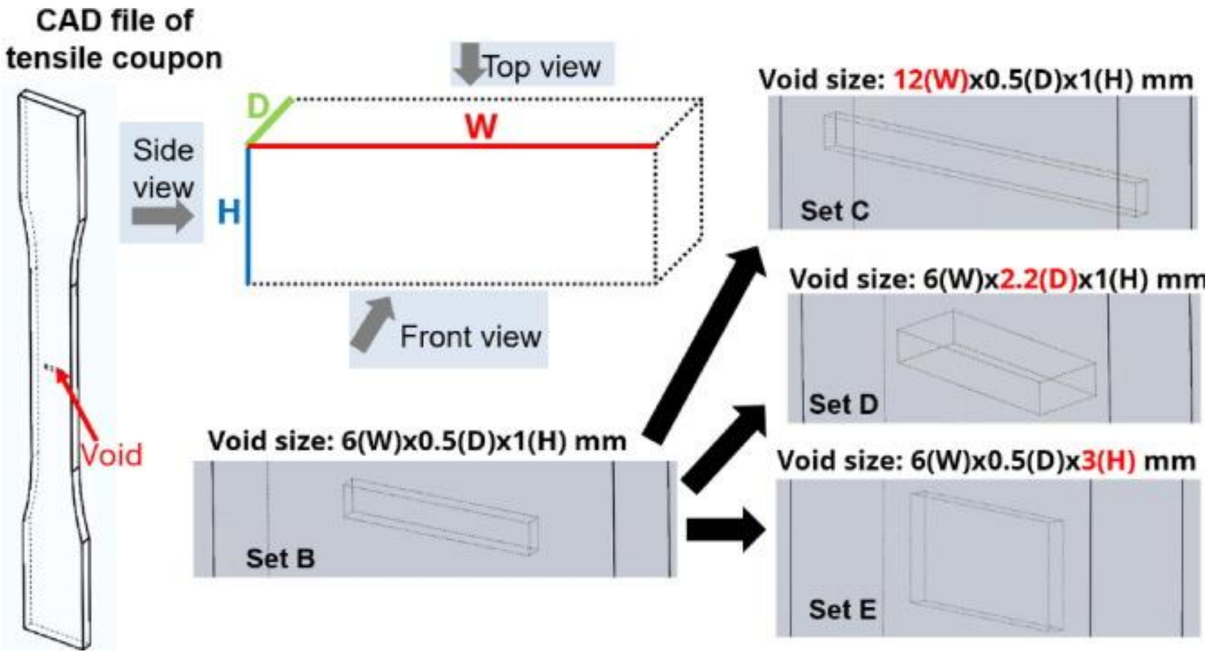

Fig. 1. CAD file of defective tensile test coupons of Set B – Set E.

2.2. Introduction of defects (voids) in ABS tensile test coupons

Defect in the form of void was used in this study, Table 1 specified the different nominal sizes of voids introduced in the tensile test coupons. 6 sets of samples (Set A to Set F) with different nominal void sizes were introduced in the tensile test coupon to determine the effects of different void sizes on the resultant Z-strength properties. Set A shown in Table 1 defined a non-defective test coupon without any introduction of void in the STL file. Set B was a controlled defective sample which possessed an introduced void at the center of tensile test coupon (refer to Fig. 1 for defect location), with a depth of 0.5 mm, width of 6 mm, and height of 1 mm in the STL file. The introduced void sizes of tensile test coupon in sets C, D, and E were based on set B, however the width, depth and height were increased to 12, 2.2, and 3 mm, respectively. Tensile test coupon set F was designed to study the combined effects of different void sizes on the Z-strength of the printed part, all 3 void sizes of sets C, D, and E were introduced to the coupons of set F spaced out equally along the tensile coupon.

Table 1. Void sizes of different sample sets.

Classification	**Nominal void size (mm)**		
	Depth	**Width**	**Height**
Set A	0	0	0
Set B	0.5	6	1
Set C	0.5	12	1
Set D	2.2	6	1
Set E	0.5	6	3
Set F	Combination of set C, D, E		

2.3. 2D X-ray imaging & analysis of tensile test coupons

2D X-ray imaging of the 3D printed tensile test coupons was performed using the GE Nano/micro X-ray CT machine (Phoenix v|tome|x m). The machine is equipped with two open X-ray sources: 180 kV open transmission tube and 240 kV reflection tube. Since the tensile coupon material used in this study is polymeric based with sample thickness of 3.2 mm, the 180 kV tube was used. A tube voltage of 100 kV, tube current of 50 μA, magnification of 10x and resolution of 10 μm was used for all 2D X-ray imaging. The 2D X-ray scanned images were processed by ImageJ and converted to 8-bit images with grayscale values ranged between 0 and 255. The regions with grayscale value between 207 and 234 of each scanned images were highlighted in red to indicate low density or thin regions which were defined as void defects.

2.4. Tensile test of 3D printed test coupons

The 3D printed test coupons with and without defects were printed according to ASTM D638 Type I dimension. The cross-sectional area of the samples in each sample set (*n* = *6*) were measured using a vernier caliper and loaded onto an Instron 5982 testing machine, where testing was conducted using 10 kN load and crosshead speed of 5 mm/min. A gauge length of 50 mm and a video extensometer for high accuracy strain measurement was used. All testing was carried out at ambient temperature. Strain was determined from the extensometer; stress was calculated as the load normalized to initial cross-sectional area.

2.5. Optical analysis of 3D printed test coupons

The cross-sectional views of fractured surfaces of the tensile samples were characterized by using an optical microscope (Olympus SZ61). All optical images were processed and analysed using ImageJ software.

3. Results & discussions

3.1. Characterization of void defects by destructive test

Various void sizes were introduced to the tensile test coupons to determine the effectiveness of 2D X-ray imaging in capturing defects. This is necessary for the development of part acceptance criteria model where an acceptable zone with satisfactory mechanical properties will be defined and use for quality check. Prior to that, it is necessary to ensure that the embedded void in STL file is correctly replicated by the printing process, hence destructive test on controlled defective tensile coupons (Set B – Set E) were conducted. The 3D printed test coupons were cryo-fractured and imaged under an optical microscopy. Fig. 2 presents the cross-sectional macroscopic front and side image of the tensile coupons' void sizes. Their respective measured versus nominal dimension on 4 different samples were presented in Fig. 2. It can be seen that all void defects were introduced into the printed structures successfully. The introduced voids had measured dimensions similar to their nominal values. Specifically, for a nominal size defect of 0.5 × 6 × 1 mm in Set B, had a measured depth of 0.59 mm, a measured width of 5.79 mm, and a measured height of 0.94 mm. For the introduced voids in Set C the measured depth, width, and height of 0.53 mm, 12.17 mm, and 0.90 mm, correspond to the nominal dimension of 0.5, 12, and 1 mm, respectively. Similarly, the measured dimension of the introduced voids of Set D and Set E were 2.27 × 6.18 × 0.93 mm and 0.67 × 5.84 × 3.07 mm, respectively, which were relatively similar to their nominal dimensions of 2.2 × 6 × 1 mm and 0.5 × 6 × 3 mm. Taken together, the embedded voids were well replicated by the FDM process, and the measured voids sizes will be taken for further studies on acceptance criteria model development.

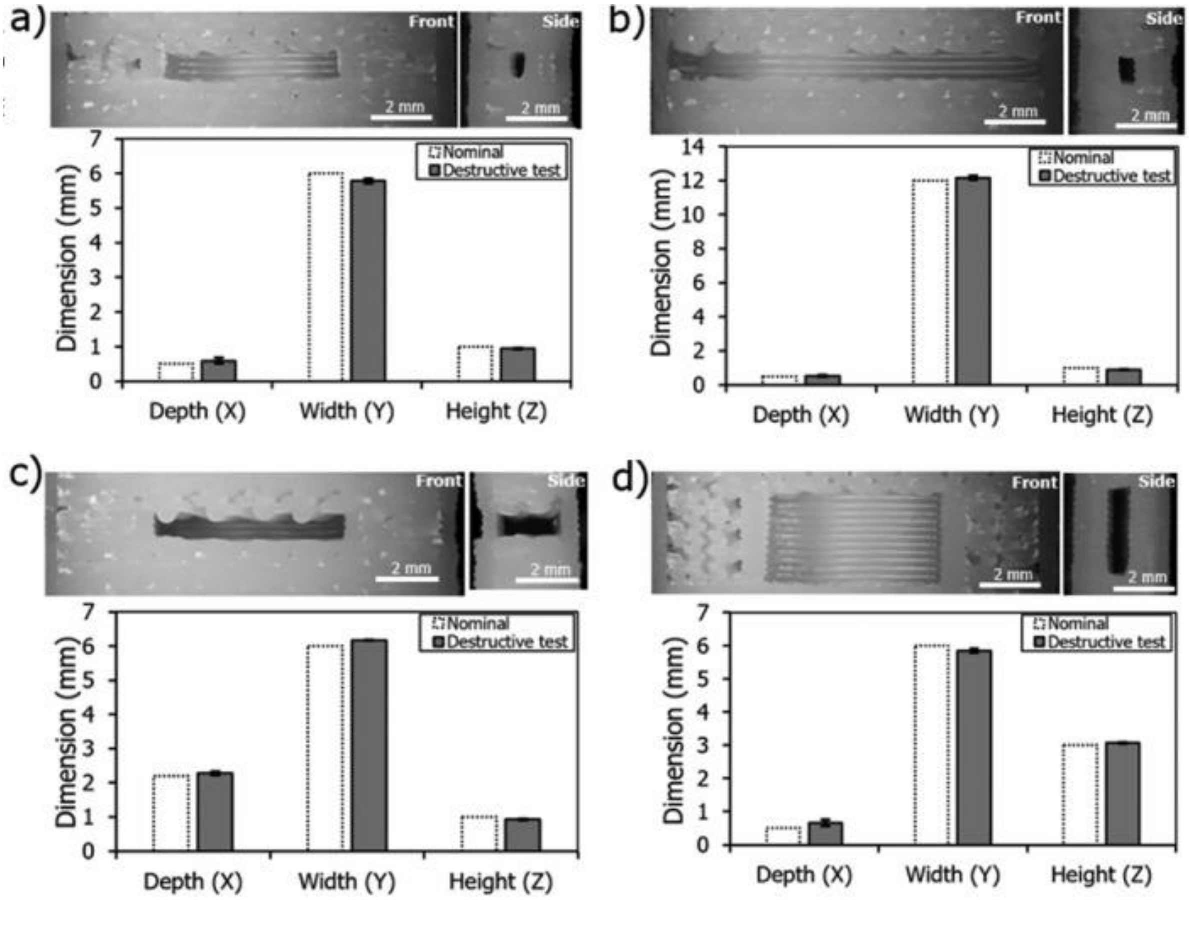

Fig. 2. Cross-sectional views of voids (front and side) with measured versus nominal dimensions in a) set B, b) set C, c) set D and d) set E.

3.2. X-ray imaging of 3D printed tensile test coupons

Fig. 3 presents the images of the printed tensile test coupons and their corresponding 2D X-ray scanning images after being processed by ImageJ. The red dots defined the grayscale value between 207 and 234 on ImageJ which were considered as less dense region hence the void defects. From Fig. 3b, there is a uniform distribution of red dots observed in all regions of set A coupons. These voids can be correlated to the inherent voids contributed by the internal inter-raster which was widely reported in FDM printed structures [4]. The coupons in the other sets, e.g., Set B to Set F, also possessed similar inherent inter-raster voids spreading uniformly in their structures as shown in Fig. 3b. However, in addition to that, significantly darker red regions were observed in set B to set E at the center of the coupons. These regions can be interpreted as being significantly thinner as a result of the introduced void defects.

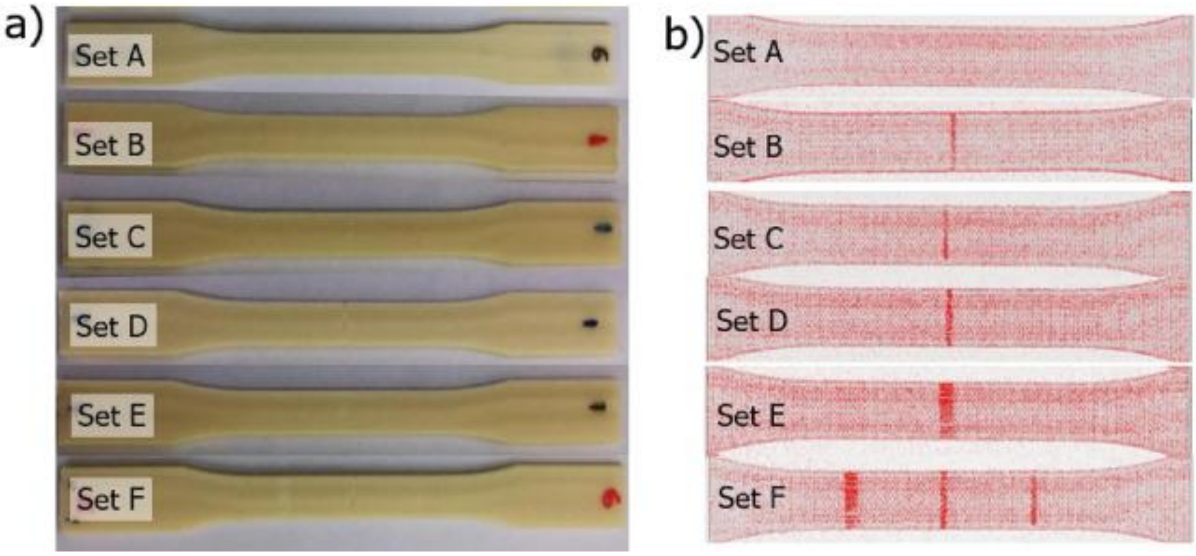

Fig. 3. a) Images of tensile coupons and b) their respective 2D X-ray scanning images processed by ImageJ.

Therefore, it can be concluded that the ImageJ analysis are consistent with the aforementioned voids embedded and observed in the destructive test. This suggest that 2D X-ray scanning in combination with ImageJ analysis is capable of capturing void defects and can be used as a non-destructive test to detect void defects.

However, while the void size of set C was similar to the nominal dimension of their introduced voids, the 2D X-ray imaging detected void width of the introduced voids in set B, D, and E was nearly twice more than that of their nominal values. The results indicate that together with the introduced voids generated by modifying the STL files of the coupons, there were additional voids at the middle regions of the coupons. These additional voids were observed at the regions next to the introduced voids, refer to Fig. 4b, d, and e, which might be formed by the modified toolpath due to the introduced voids in the STL files. As presented in Fig. 5, the toolpaths of set A and set C were more continuous with less inter-raster voids formation, whereas less continuous with more small regions and inter-raster voids could be observed in the toolpaths of sets B, D, and E. Consequently, the ABS melt in the printing process of sets B, D, and E might not be deposited properly at these regions, leading to the formation of additional voids seen in Fig. 4.

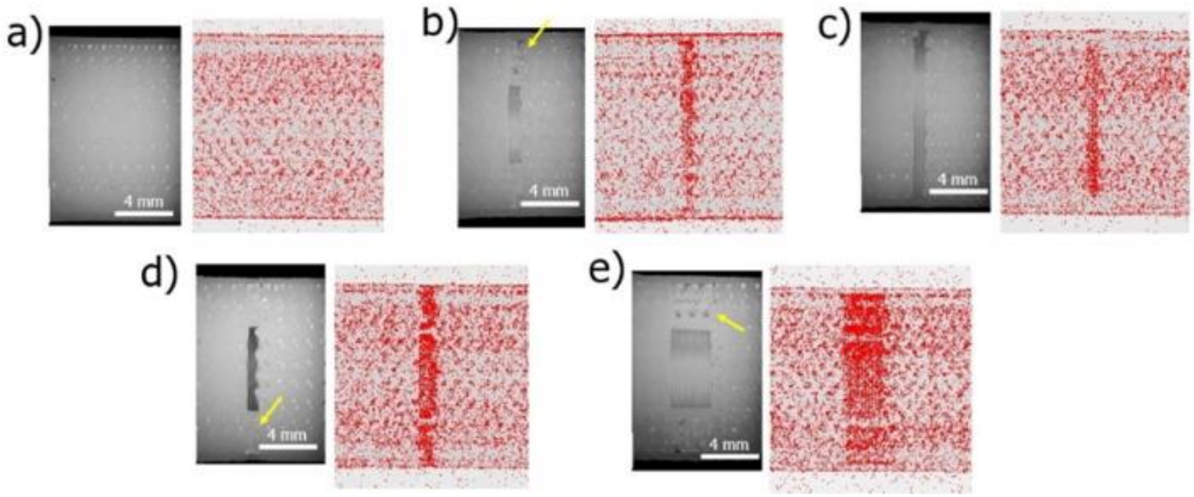

Fig. 4. Cross-sectional (Front view) and corresponding 2D X-ray images of voids introduced in a) set A, b) set B, c) set C, d) set D, and e) set E.

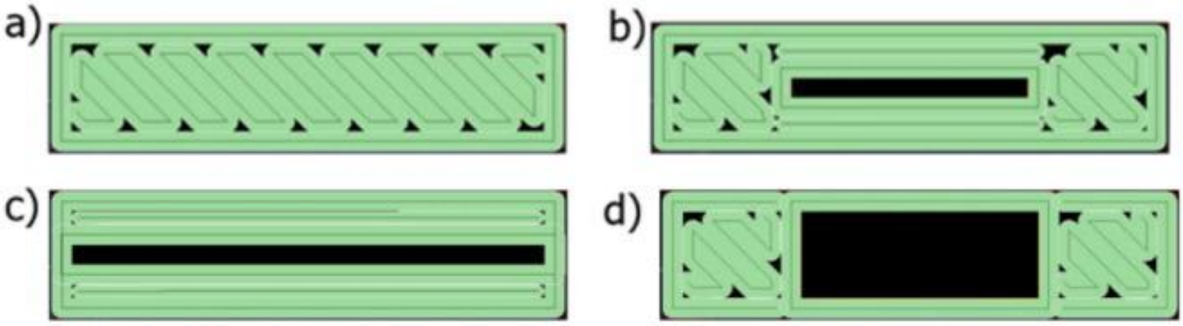

Fig. 5. Tooth path of melt deposition at the middle layer of tensile coupons in a) set A, b) set B and E, c) set C, and set D.

3.3. Mechanical stress analysis of 3D printed coupons

Fig. 6 present the stress–strain curves, fractured tensile samples, and compiled mechanical strength data of the 3D printed test coupons. As can be seen, all tensile tests were valid with samples breaking within the gage length. Samples of set A had no introduced void defect and, therefore, broke at random positions within the gage length. All samples of the other sets, however, broke at the center of their gagelength where the introduced void defects act as stress risers. The mechanical performance of defect-free set A coupons was the highest with a maximum tensile strength of 22.6 ± 0.48 MPa, Young's modulus of 1.88 ± 0.04 GPa, and strain at break of 0.019 ± 0.002. However, the coupons of set B had 25.4 % lower in tensile strength, 4.8 % lower in Young's modulus, and 37.4 % lower in strain at break as compared to set A. This reduction in strength was expected as the additional void defects in the printed coupons of set B weakened their strucutre and lowered their mechanical performance.

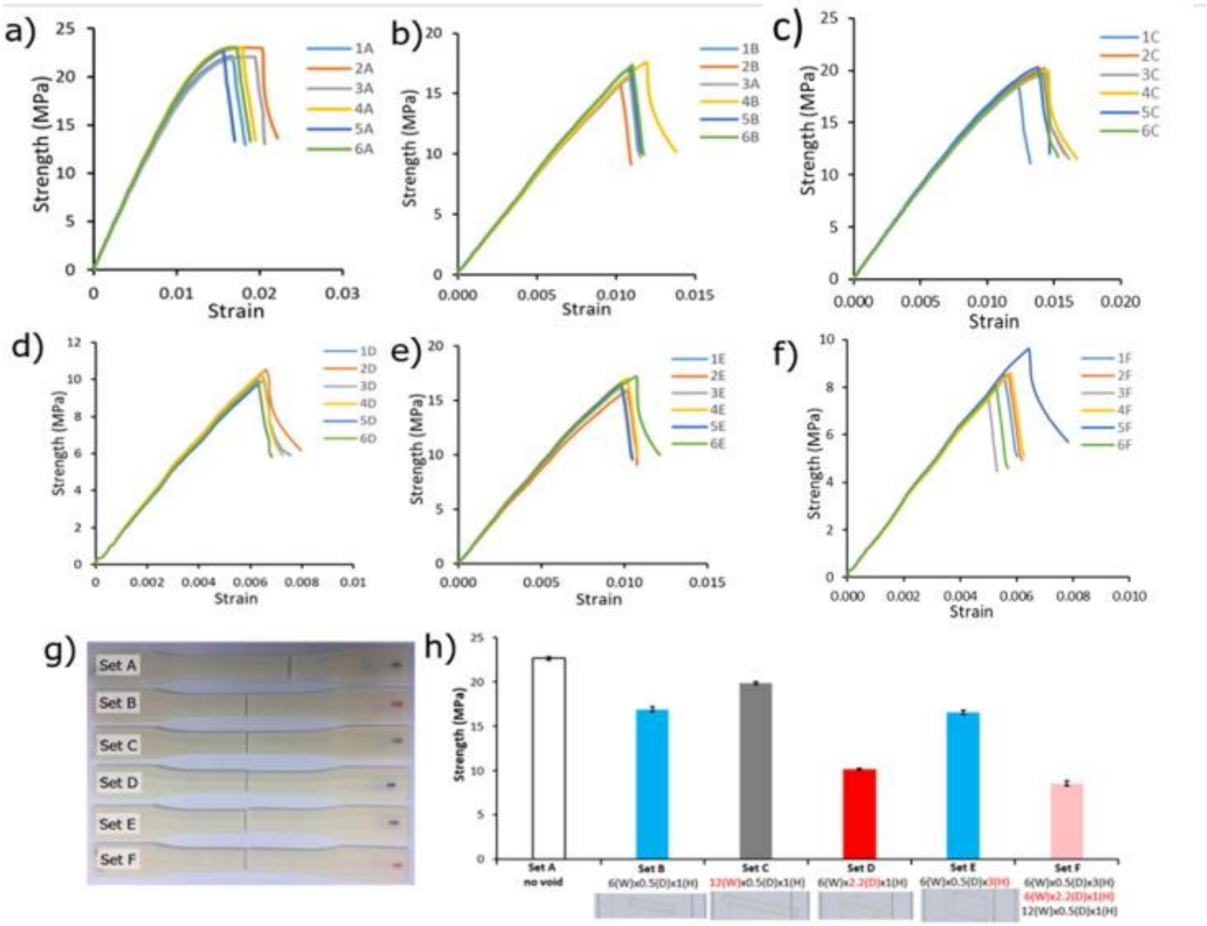

Fig. 6. a – f) Stress–strain curves of set A to set F respectively; g) Fractured samples of set A to set F; and h) compiled tensile strength of set A to set F.

Compared to coupons of set B, the samples of sets C, D, and E possessed larger void defects in width, depth, and height, respectively, and, therefore, their differences in mechanical performance could offer their correlation with the dimension of the void defects. As can be seen, coupons of set D had the lowest mechanical performance with 40 % lower in maximum tensile strength, 4.9 % lower in Young's modulus, and 36.2 % lower in strain at break compared to set B. The mechanical properties of Set C coupons, however, were better than those of the samples in set B. Although their Young's modulus was slightly lower, their tensile strength, and strain at break were 19.9 MPa, and 0.016 respectively, which was 17.5 %, and 33.5 % higher than those of set B coupons, respectively. Interestingly, there were insignificant differences in the mechanical performance between the tensile coupons of set E and set B. This might be due to the fact that both sets had the same in-plane cross-sectional areas at the middle of the coupons. Additionally, their toolpath of the coupons were similar, leading to the formation of additional voids with similar configuration at the regions near the introduced voids. This findings suggest that the void height had no remarkable influences on the mechanical properties of the printed samples in Z direction. For sample Set C & D the defect size at the cross-sectional area perpendicular to load direction is greater than set B & E therefore a lower mechanical properties can be expected. However, this is not the case for sample C, notably, the effects of void defects on the mechanical properties were complicated due to additional voids formed by the inefficient deposition of ABS melts at the narrow modified toolpath regions. Therefore, it is necessary to critically define the cross-sectional fracture area to develop the accpetance criteria model.

3.4. Correlation between void characteristics and Z-strength of the printed parts

Fig. 7a-d shows the fracture surfaces and the whitening area of tested coupons of set A, B, C, and D as indicated with red arrows. Set E has been omitted in this study as the in-plane cross-sectional area and tensile strength is similar to set B. As can be seen from the images, all fracture surfaces exhibited stress whitening effect which is due to the internal stress generated during the tensile testing process. The white areas were, therefore, the regions where ABS raster interfaces were diffused and bonded together. By using ImageJ to extract the whitening areas, their fraction and void area fraction could be determined and is presented in Table 2. As can be seen, the coupons of Set A possessed the densest structure, evidenced by the highest whitening area fraction (84.32 %) and the lowest void area fraction (15.68 %). As there were no voids introduced to their STL files, these voids area fraction were the measured fraction of inherent inter-raster voids of the printed samples. Due to the introduction of voids in the STL file, the whitening area fraction of Set B coupons were 27 % lower than that of the set A coupons, corresponding to a void area fraction of 38.41 %. The whitening area fraction of Set

D were the lowest (36.65 %), leading to a void area fraction of 63.35 %. Interestingly, although the void introduced to the STL file of set C coupons were larger than that of set B coupons, their whitening area fraction was slightly higher (69.92 %), resulting in a 21.7 % lower in void area fraction. The findings are consistent with the aforementioned results obtained from their 2D X-ray scanned images and cross-sections, suggesting that additional voids were formed next to their introduced voids due to modified toolpaths.

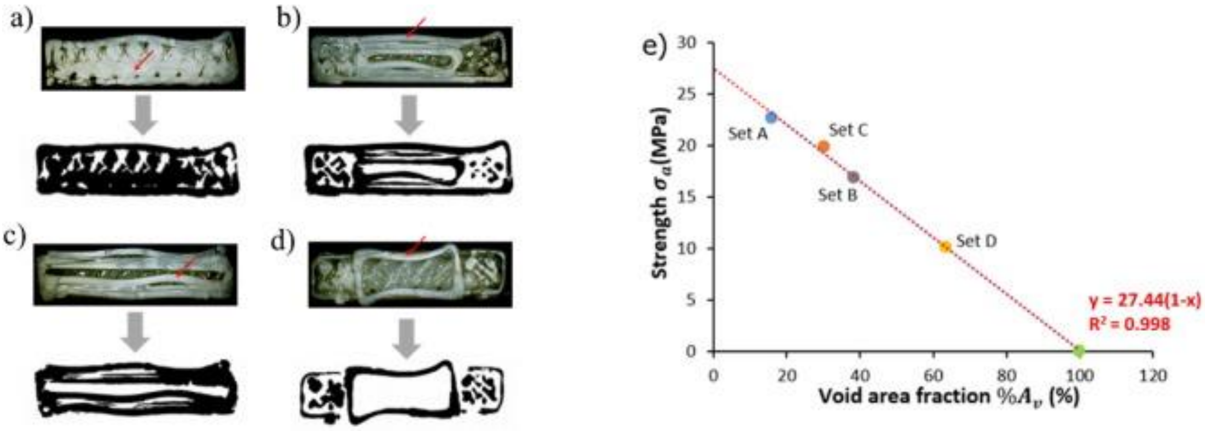

Fig. 7. a) Fractured surfaces and the corresponding whitening areas (red arrow) of tensile coupons of a) set A, b) set B, c) set C, and d) set D. e) Correlation between void area fraction and Z-strength of the printed tensile coupons. (For interpretation of the references to colour in this figure legend, the reader is referred to the web version of this article.)

Table 2. Area fraction and strength of different tensile test coupons.

Classification	**Whitening area fraction (%)**	**Void area fraction (%)**	**Strength (MPa)**
Set A	84.32	15.68	22.65 ± 0.48
Set B	61.59	38.41	16.89 ± 0.66
Set C	69.92	30.08	19.86 ± 0.43
Set D	36.65	63.35	10.12 ± 0.29
Set F	0	100	0

Fig. 7e plots the tensile strength of the tensile coupons versus void area fraction. As can be seen, a linear correlation with equation of y = 27.44(1-x) was generated between the two parameters with linear regression of $R^2 = 0.998$. A lower limit was set for 100 % void fraction areas to ensure the correlation was more accurate. The good linear agreement seen in this model could be due to the use of highly ductile ABS material. Ductile material like ABS usually exhibit more stress absorption beyond its yield strength hence lesser unpredictable failure and more consistent tensile strength results [6], however brittle material might not present similar trend. From the correlation studies seen in Fig. 7e, the plot of tensile strength versus void area fraction could be generated for other feedstock materials by determining the values of set A, a few embedded defect sample sets and the lower limit to obtain the correlation model.

For quality control checks related to a minimum tensile strength requirement, the correlation model could be used to determine the maximum allowable values for void area fractions as acceptance criteria. It also could be used to estimate the tensile strength of the printed parts at the void regions to predict the stress concentration areas and possible failure positions. The acceptable zone could be formed according to the required mechanical strength defined by quality control requirement, as shown in Fig. 8.

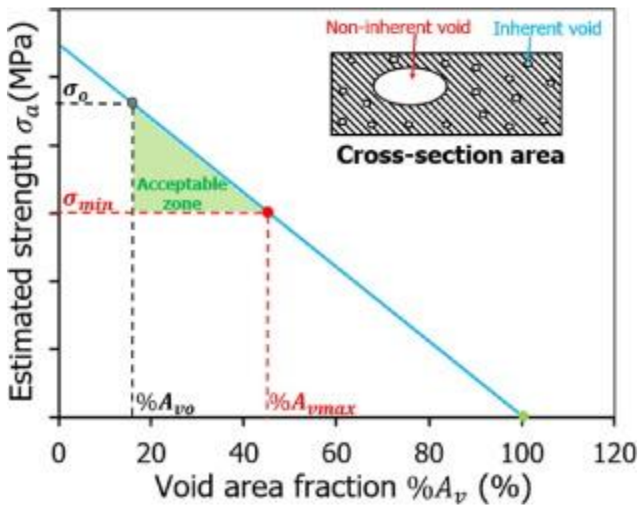

Fig. 8. Acceptance criteria model for quality control of FDM printed samples.

4. Conclusion

An acceptance criteria model for the quality control checks of FDM printed part has been developed in this study which employed the cheaper and faster 2D X-ray NDI technique. Preliminary studies suggest that 2D X-ray imaging is capable of detecting controlled embedded voids in FDM printed parts. Good linear agreement has been observed between the 3D printed cross-sectional void content and its respective tensile strength. This suggest the possibility of using such model for quality control checks. Taken together, the developed methodology provides FDM user a faster, greener and more efficient NDI technique compared to the conventional 3D micro-CT scan. While this study uses voids and tensile coupons as demonstrator, the methodology outlined here can be further studied for other sub-surface defects and material system.

CRediT authorship contribution statement

Feng Lin Ng: Conceptualization, Supervision, Writing - original draft, Writing - review & editing. **Thang Q. Tran:** Investigation, Conceptualization, Methodology, Writing - original draft. **Tong Liu:** Investigation.

Declaration of Competing Interest

The authors declare that they have no known competing financial interests or personal relationships that could have appeared to influence the work reported in this paper.

Acknowledgements

This work is supported by the Singapore Institute of Manufacturing Technology (SIMTech), A*STAR, Singapore.

References

[1] Alba Cano-Vicent, Murtaza M. Tambuwala, Sk. Sarif Hassan, Debmalya Barh, Alaa A. A. Aljabali, Martin Birkett, Arun Arjunan, Ángel Serrano-Aroca. Fused deposition modelling: Current status, methodology, applications and future prospects. Addit. Manuf. 2021, 47, 102378.

[2]T.Q. Tran, F.L. Ng, J.T.Y. Kai, S. Feih, M.L.S. Nai. Tensile strength enhancement of fused filament fabrication printed parts: a review of process improvement approaches and respective impact. Addit. Manuf. 2022, 54, 102724

[3] A. Hernandez-Contreras, L. Ruiz-Huerta, A. Caballero-Ruiz, V. Moock, H.R. Siller Extended CT void analysis in FDM additive manufacturing components. Materials 2020, 13, 3831

[4] Bartosz Gapiński, Michał Wieczorowski, Mirosław Grzelka, Pedro Arroyo Alonso, Adrián Bermúdez Tomé. The application of micro computed tomography to assess quality of parts manufactured by means of rapid prototyping. *Polimery* 2017, 62, 53-59.

[5] M.R. Khosravani, T. Reinicke. On the use of X-ray computed tomography in assessment of 3D-printed components. J. Nondestruct. Evaluat. 2020, 39, 75

[6] M.D. Hayes, D.B. Edwards, A.R. Shah. Fractography in Failure Analysis of Polymers. William Andrew, New York (2015).